

# Spin currents in rough graphene nanoribbons: Universal fluctuations and spin injection

Michael Wimmer,<sup>1,\*</sup> İnanç Adagideli,<sup>1,\*</sup> Savas Berber,<sup>1,2</sup> David Tománek,<sup>2,1</sup> and Klaus Richter<sup>1</sup>

<sup>1</sup>*Institut für Theoretische Physik, Universität Regensburg, D-93040, Germany*

<sup>2</sup>*Department of Physics and Astronomy, Michigan State University, East Lansing, Michigan 48824-2320, USA*

(Dated: October 31, 2018)

We investigate spin conductance in zigzag graphene nanoribbons and propose a spin injection mechanism based only on graphitic nanostructures. We find that nanoribbons with atomically straight, symmetric edges show zero spin conductance, but nonzero spin Hall conductance. Only nanoribbons with asymmetrically shaped edges give rise to a finite spin conductance and can be used for spin injection into graphene. Furthermore, nanoribbons with rough edges exhibit mesoscopic spin conductance fluctuations with a universal value of rms  $G_s \approx 0.4e/4\pi$ .

PACS numbers: 85.75.-d 73.63.-b 72.25.-b 73.22.-f

After their experimental discovery in 2004 [1], monolayers of graphite have attracted much experimental and theoretical attention owing to their unusual band structure [2]. Graphene has also been suggested as a good candidate for spin based quantum computing and spintronics [3], as it is expected to have long spin decoherence/relaxation times [4]. This prospect led to the recent interest in generating and manipulating net spin distributions in graphene. Recently, spin injection from ferromagnetic metal contacts into graphene has been achieved [5, 6, 7, 8].

Transport properties of graphene nanoribbons (GNR) are expected to depend strongly on whether they have an armchair or zigzag edge [9]. In GNRs with zigzag edges, transport is dominated by edge states which have been observed in scanning tunneling microscopy [10]. Moreover, owing to their high degeneracy, these states are expected to be spin polarized [11], making zigzag GNRs attractive for spintronics [12]. In addition, edge states are expected to occur also in nanoribbons with other edge orientations [13]. Recently, the first transport experiments have been performed in narrow ribbons of graphene [14], albeit with not well defined edges. Recent theoretical work focused on charge transport through rough GNRs [15], but spin transport properties have not been explored yet.

In the present work, we focus on spin transport in GNRs with rough zigzag edges. Ideal zigzag GNRs are not efficient spin injectors due to the symmetry between the edges with opposite magnetization. In order to obtain net spin injection, this symmetry must be broken. Existing proposals to achieve this require very large transverse electric fields [12]. We sidestep this difficulty by showing that edge imperfections (such as vacancies), which usually cannot be avoided experimentally, break the symmetry between the edges and lead to a finite spin conductance of the GNR. Thus, rough zigzag GNRs can be used as spin injectors or detectors in graphene spintronics.

We start with a description of the electronic ground state properties of the zigzag GNR, which captures the

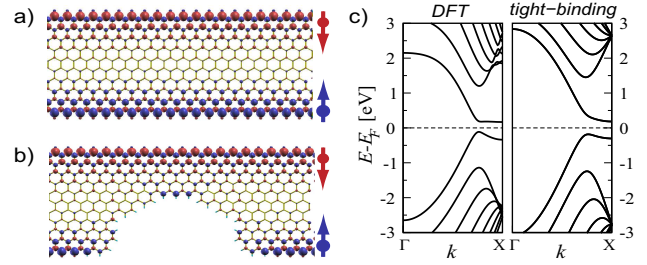


FIG. 1: (color online) Ground state spin density for (a) an ideal and (b) an imperfect zigzag GNR. Blue (red) corresponds to up (down) spin density. (c) Band structures of an ideal GNR obtained from DFT and tight-binding approaches.

essential physics relevant to spin transport, given by the single band tight-binding Hamiltonian [11]

$$H = \sum_{ij,s} t_{ij} c_{i,s}^\dagger c_{j,s} + \sum_{i,s,s'} \mathbf{m}_i \cdot c_{i,s}^\dagger \boldsymbol{\sigma}_{s,s'} c_{i,s'}. \quad (1)$$

Here  $t_{ij} = t$  if  $i$  and  $j$  are nearest neighbors,  $t_{ij} = t'$  if  $i$  and  $j$  are next nearest neighbors [16], and  $\boldsymbol{\sigma}$  are the Pauli matrices corresponding to the spin degree of freedom. The local magnetization  $\mathbf{m}_i$  can be obtained from the self consistency condition or *ab initio* calculations.

Our *ab initio* results, obtained using the spin-polarized density functional formalism (DFT) [17], agree with the reported finding [11, 12, 18] that the local magnetization is staggered in the electronic ground state, as shown in Fig. 1(a). At zero doping the antiferromagnetic (AF) ordering generates a gap in the single particle spectrum. We now dope the GNR in order to move into a regime with open conduction channels. This can be achieved in practice by applying a gate voltage or chemical doping. Our DFT results indicate that a finite amount of doping reduces the AF gap and the local magnetization, but does not destroy the AF ordering. We obtain the critical value of this doping as  $\approx 0.5$  electrons ( $\approx 0.4$  holes) per zigzag edge atom. Furthermore, our DFT calculations show that not only perfect, but also rough zigzag rib-

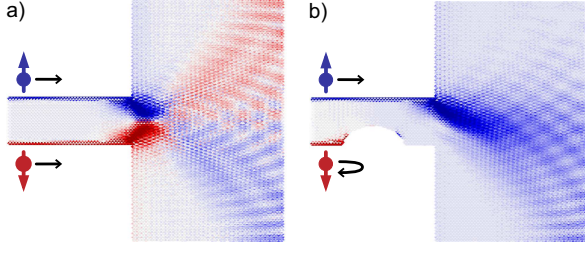


FIG. 2: (color online) Spin injection profile from (a) an ideal GNR and (b) a GNR with a distorted edge into a region of n-doped graphene. Nonequilibrium densities for spin up (down) electrons are shown in blue (red).

bons exhibit spin polarization (Fig. 1(b)). In addition, the formation of multiple spin domains at zigzag edges is energetically prohibitive. In summary, our DFT calculations show that it is possible (i) to dope the GNR to make them conductive and (ii) to introduce disorder at the edges while retaining the magnetic ordering.

Next, we further simplify the mean field description of Eq. (1) by ignoring the variation of  $\mathbf{m}_i$  within a sublattice. A spatial dependence of  $\mathbf{m}_i$  changes the amount of band dispersion, modifying the energy window, within which the transport predominantly involves the edge states. This leads to the single particle Hamiltonian

$$H_{mf} = \epsilon(k)\tau_1 + \Delta(k)\tau_2 + A(k)I + \mathbf{m} \cdot \boldsymbol{\sigma}\tau_3, \quad (2)$$

where  $\epsilon(k)$ ,  $\Delta(k)$  and  $A(k)$  are obtained by Fourier transforming Eq. (1), and  $\tau_i$  are the Pauli matrices corresponding to pseudospin(sublattice) degrees of freedom [19]. The AF exchange field  $\mathbf{m}$  is obtained by fitting the band structure to DFT results (see Fig. 1(c)).

In the following, we focus on transport properties of the GNR. We work in the linear response regime so that all the transport properties of the GNR are specified by the effective single-particle Hamiltonian (2). The spin conductance [20] of a GNR is given by  $G_s = (e/4\pi)(T_\uparrow - T_\downarrow)$ , where  $T_{\uparrow(\downarrow)}$  is the transmission probability for spin up (down). The conducting channels with energies closest to the Fermi energy of the undoped system reside on a single sublattice and are fully spin polarized owing to the staggered magnetization. These states are extended along the ribbon axis, but localized near the (zigzag) edges, with the spin up channel localized at one edge and the down channel on the opposite edge. The transverse localization length of these states depends on their Fermi momentum  $k_F$  that may be modified by shifting the Fermi energy  $E_F$ . As one moves away from the X point, the transverse localization length increases as  $\lambda_{\text{edge}} \approx -a/\ln(2\cos(k_F a/2))$ , where  $a = 2.46 \text{ \AA}$  is the hexagonal lattice constant [11]. Owing to the spatial separation of the edge states, the scattering of spin up and spin down carriers occurs only at the edge, where they reside, and is unaffected by the opposite edge. Distinguishing a left (l) and right (r) edge of the nanoribbon, we

approximate  $T_{\uparrow(\downarrow)}$  by  $T_{l(r)}$ , where  $T_{l(r)}$  is the transmission probability of the corresponding edge state, assuming the opposite edge is not disordered. The transport properties of the zigzag GNR are thus essentially those of two independent wires, oppositely spin polarized and connected in parallel between the reservoirs. We note that previous studies of edge state transport [21] assumed vanishing next nearest neighbor hopping  $t'$ , and obtained results in apparent contradiction to the picture presented above: If  $t'$  were zero, the charge density would be localized at the edges, but the current density would be extended through the GNR. This leads to the incorrect conclusion that edge states would scatter equally from impurities at *both* edges. In reality, the edge states show non-zero dispersion (such as due to  $t' \neq 0$ ). In this case, the current flow is also localized at the edges [22] validating the two-wire model, as we show below.

For an ideal, impurity-free GNR, we have  $T_l = T_r$ , which leads to vanishing spin conductance. This is confirmed by quantum transport simulations [23] and an illustrative example is shown in Fig. 2(a): Both edge channels transmit equally. However, as the edge states enter the bulk graphene, they are deflected: In the GNR, the pseudospin is predominantly in  $z$ -direction and tied to the electron spin, whereas in the bulk pseudospin is in-plane and tied to the current direction. At the interface, the  $z$ -component splits into states with positive and negative velocity perpendicular to the boundary. The state with velocity towards the boundary is scattered [22] and thus, upon entry, states at opposite edges (which carry opposite spins) deflect in opposite directions, leading to a finite spin Hall conductance (Fig. 2(a)). Finite spin conductance can be obtained, however, for imperfect GNRs: An obstacle scatters the spin channel localized at the same edge more effectively, leading to a non-vanishing spin conductance and spin injection (Fig. 2(b)). Whereas the efficiency of the spin Hall effect is limited by the mean free path, and thus ballistic microstructures are needed to observe it, the efficiency of spin injection with edge defects is limited only by the spin relaxation length and can be used to inject spins into diffusive systems.

From an experimental perspective, unless the GNRs are specifically fabricated with edges of different roughness, the average conductance of both spin channels is equal, quenching the ensemble-averaged spin conductance. Yet, in the mesoscopic regime, sample-to-sample fluctuations of  $T_{\uparrow,\downarrow}$  lead to a non-vanishing variance of the spin conductance. In the two-wire model we have

$$\text{Var } G_s = \left(\frac{\hbar}{2e}\right)^2 \text{Var } G_{\text{tot}} = \left(\frac{e}{4\pi}\right)^2 (\text{Var } T_l + \text{Var } T_r).$$

Treating both edges as one-dimensional wires, we map the transport problem onto that of a disordered 1D chain. Transmission eigenvalue statistics in 1D disordered chains is known to be described by the Dorokhov-Mello-Pereyra-Kumar (DMPK) equation [24]. Using the

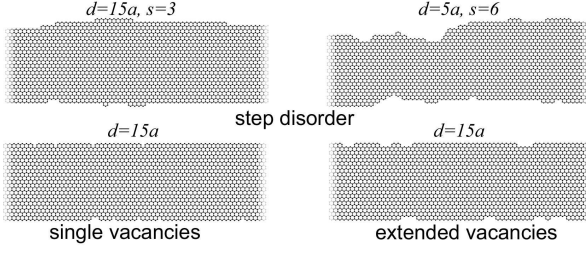


FIG. 3: Step disorder: edge disorder created by a random walk, where the width of the nanoribbon is changed by one hexagon at every step. Steps are made with probability  $a/d$  and the maximum deviation of the width is  $\leq s$  hexagons. Single vacancies: edge atoms are removed randomly with the probability  $a/d$ . Extended vacancies: similar to single vacancies, but also neighboring edge atoms are removed.

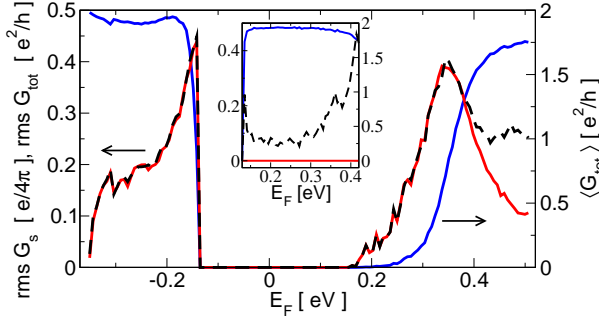


FIG. 4: (color online) Average total conductance,  $\langle G_{\text{tot}} \rangle$  (blue solid line), rms of the total conductance,  $\text{rms } G_{\text{tot}}$  (black dashed line), and rms of the spin conductance,  $\text{rms } G_s$  (red solid line), as a function of  $E_F$  ( $E_F = 0$  is chosen to correspond to zero gate voltage). The data were averaged over 1000 configurations of single vacancies with  $d = 40a$  and  $L = 800a$ . For comparison, the inset shows the same quantities for the singular case of  $t' = 0$ . In this situation, the spin conductance and its fluctuations vanish completely.

full distribution function of resistance [25], we find that the universal maximum value of the root mean square (rms) spin conductance  $\text{rms } G_s = \sqrt{\text{Var } G_s} \approx 0.4e/4\pi$ . In order to demonstrate this universality, we investigate GNRs of different length  $L$  and width  $W$  and various models of edge disorder (see Fig. 3).

First, we focus on dilute disorder, where the average distance between scatterers  $d \gg a$ . The typical behavior of charge and spin conductances (average, fluctuations) is shown in Fig. 4. We first note that over the whole energy region, where the edge states are present,  $\frac{\hbar}{2e} \text{rms } G_{\text{tot}} \approx \text{rms } G_s$ , confirming the validity of the two-wire model. As the Fermi level is raised by gating or doping, the relevant states are extended and feel both edges. Then, the assumption of uncorrelated channels breaks down, and  $\frac{\hbar}{2e} \text{rms } G_{\text{tot}} > \text{rms } G_s$ .

For an n-type GNR, when the Fermi level is near the band edge, the states at  $E_F$  are localized and both the average conductance and the fluctuations are sup-

pressed exponentially. Raising  $E_F$ , we observe in Fig. 4 a crossover to the ballistic regime, where the conductance rises up to the quantum limit of conductance  $2e^2/h$ . Correspondingly, we see a maximum in the conductance fluctuations before they vanish again in the ballistic regime.

The average/fluctuations of the conductances of a p-doped GNR are different from an n-doped one, but a description based on the DMPK equation holds well for either case. The scattering strength of impurities depends on the overlap of the impurity potential with the unperturbed channel wavefunction and therefore on  $\lambda_{\text{edge}} = \lambda_{\text{edge}}(E_F)$ . In the n-doped GNR, there is one channel whose momentum is a monotonic function of  $E_F$ . On the other hand, in the p-doped GNR, due to the band dispersion (Fig. 1), there are two channels: One localized near the edge, the other extended further into the ribbon, but still with a considerable density at the edge. Lowering  $E_F$  thus localizes one state even more towards the edge, whereas the other state spreads out, making the density more uniform. This leads to different functional dependences of the localization length on the Fermi energy for n- and p-doped ribbons.

In order to compare n- and p-doped ribbons as well as different disorder models, we extract the energy dependence of the longitudinal (transport) localization length  $\xi(E_F)$  from  $\exp(\langle \ln(G_{\uparrow/\downarrow}(E_F, L)) \rangle) = \exp(-2L/\xi)$  [26, 27], as shown in the inset of Fig. 5(a). In Fig. 5(a) we show  $\text{rms } G_s$  as a function of  $\xi/L$  for all three disorder models (see Fig. 3) with different values of  $d$  and a wide range of ribbon lengths  $L$ . The data collapse onto a single curve, demonstrating the universality of the spin conductance fluctuations (SCF), independent of the particular type of edge disorder. Slight deviations from this universality can be observed in Fig. 5(a), in the ballistic regime for the special case of single vacancies. In this case, the system reaches the ballistic limit only for high Fermi energy values, where the two-wire model breaks down. The rms spin conductance of the n-doped GNR agrees very well with the results obtained from the DMPK equation. For the p-doped ribbon, where there are two conducting channels, we see a small increase in the rms conductance, presumably due to the crossover to a multi-channel quasi-1D wire, where  $\text{rms } G \approx 0.52$  [27]. In Fig. 5(b) we concentrate on n-doped graphene for step disorder (upper panels of Fig. 3) and show again the universality of the SCF with respect to a wide range of parameters characterizing edge roughness, ribbon length and width. There is little dependence on the ribbon width  $W$ , confirming that the observed effect is entirely due to the edges.

Currently there is not much experimental control over the edges of nanoribbons. Considering GNRs with dense disorder,  $d = \mathcal{O}(a)$ , the observed maximum of SCF decreases with increasing disorder density, i.e. decreasing  $d$ , as shown in the inset of Fig. 5(b). We observe that for  $d > 5a$  the SCF are independent of the maximum height of the steps. Moreover, we find that the maxi-



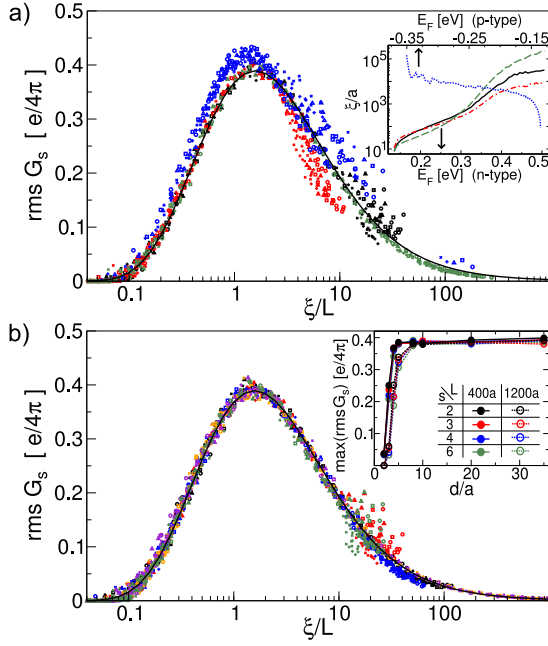


FIG. 5: (color online) Spin conductance fluctuations: (a)  $\text{rms } G_s$  as a function of  $\xi/L$  for n- and p-doped graphene: step disorder for n-type,  $d = 20a$ ,  $s = 3$  (black), single vacancies for n- and p-type,  $d = 40a$  (red and blue, respectively) and extended vacancies for n-type,  $d = 30a$  (green). Inset:  $\xi/a$  as a function of  $E_F$  for different disorder models (colors as in the main panel). (b)  $\text{rms } G_s$  as a function of  $\xi/L$  for step disorder in n-doped graphene:  $d = 20a$  and  $s = 3$  (red; orange for  $W = 92a/\sqrt{3}$ ),  $d = 35a$  and  $s = 2$  (black),  $d = 35a$  and  $s = 6$  (blue; violet for  $W = 92a/\sqrt{3}$ ),  $d = 20a$  and  $s = 6$  (green). Inset: maximum value of  $\text{rms } G_s$  as a function of  $d/a$  for the step disorder models. In both (a) and (b), the solid line corresponds to the DMPK prediction. The data is shown for GNR lengths  $L = 800a$  ( $\circ$ ),  $1000a$  ( $\square$ ),  $1200a$  ( $\triangle$ ),  $1400a$  ( $+$ ), and  $1600a$  ( $\times$ ), width  $W = 32/\sqrt{3}a$  unless specified otherwise. The  $\text{rms } G_s$  is estimated from 1000 ( $W = 32a/\sqrt{3}$ ) and 750 ( $W = 92a/\sqrt{3}$ ) disorder configurations.

imum value of the SCF is retained for  $d \gtrsim 5a$ . As an example, the system depicted in the upper right corner of Fig. 3 shows spin conductance  $\approx 0.4e/4\pi$ . The finite spin conductance of GNRs predicted above, and thus the existence of the edge state magnetism, can be detected by measuring charge conductance, e.g. by attaching ferromagnetic leads in a two- or four-probe measurement similar to Ref. [5], with one lead being a zigzag GNR.

In conclusion, we have discussed the spin transport properties of graphene nanoribbons. We have shown that an ideal GNR has zero spin conductance but nonzero spin Hall conductance. Moreover, only GNRs with imperfect edges exhibit a nonzero spin conductance. The fluctuations of the spin conductance are universal with a maximum rms conductance  $\approx 0.4e/4\pi$ . Thus, graphene nanoribbons can be used as an efficient alternative to ferromagnetic leads, paving the way to all-graphene spintronics devices.

We thank B.J. van Wees, A. Morpurgo and M. Shiraishi for discussions. I.A., M.W., S.B. and K.R. acknowledge financial support by DFG (SFB689, GRK638) and D.T. by NSF NIRT grant ECS-0506309, NSF NSEC grant EEC-425826 and the A. v. Humboldt Foundation.

\* These authors contributed equally to this work.

- [1] K. S. Novoselov *et al.*, Science **306**, 666 (2004).
- [2] A. K. Geim, and K. S. Novoselov, Nature Mat. **6**, 183 (2007); M. I. Katsnelson, Mater. Today **10**, 20 (2007); A. H. Castro Neto *et al.*, arXiv:0709.1163v1.
- [3] B. Trauzettel *et al.*, Nature Phys. **3**, 192 (2007).
- [4] H. Min *et al.*, Phys. Rev. B **74**, 165310 (2006); D. Huertas-Hernando, F. Guinea, and A. Brataas, Phys. Rev. B **74**, 155426 (2006).
- [5] N. Tombros *et al.*, Nature **448**, 571 (2007).
- [6] S. Cho, Y.-F. Chen, and M. S. Fuhrer, Appl. Phys. Lett. **91**, 123105 (2007).
- [7] E. W. Hill *et al.*, IEEE Trans. Magn. **42**, 2694 (2006).
- [8] M. Ohishi *et al.*, Jpn. J. Appl. Phys. **46**, L605 (2007).
- [9] K. Nakada *et al.*, Phys. Rev. B **54**, 17954 (1996).
- [10] Y. Kobayashi *et al.*, Phys. Rev. B **73**, 125415 (2006); Y. Niimi *et al.*, Phys. Rev. B **73**, 085421 (2006).
- [11] M. Fujita *et al.*, J. Phys. Soc. Jpn. **65**, 1920 (1996).
- [12] Y.-W. Son, M. L. Cohen, and S. G. Louie, Nature **444**, 347 (2007).
- [13] A. R. Akhmerov and C. W. J. Beenakker, Phys. Rev. B **77**, 085423 (2008).
- [14] M. Y. Han *et al.*, Phys. Rev. Lett. **98**, 206805 (2007); Z. Chen *et al.*, Physica E **40**, 228 (2007).
- [15] I. Martin and Y. M. Blanter, arXiv:0705.0532v2; F. Sols, F. Guinea, and A. H. Castro Neto, Phys. Rev. Lett. **99**, 166803 (2007); J. P. Robinson and H. Schomerus, Phys. Rev. B **76**, 115430 (2007).
- [16] P. R. Wallace, Phys. Rev. **71**, 622 (1947); K. Sasaki, S. Murakami, and R. Saito, Appl. Phys. Lett. **88**, 113110 (2006).
- [17] As implemented in SIESTA: P. Ordejón, E. Artacho, and J. M. Soler, Phys. Rev. B **53**, R10441 (1996); J. M. Soler *et al.*, J. Phys.: Condens. Matter **14**, 2745 (2002).
- [18] S. Okada and A. Oshiyama, Phys. Rev. Lett. **87**, 146803 (2001).
- [19] F. D. M. Haldane, Phys. Rev. Lett. **61**, 2015 (1988).
- [20] The unit of spin conductance is  $e/4\pi$ , in contrast to the spin-resolved charge conductance  $G_{\uparrow,\downarrow}$ , which is  $e^2/h$ .
- [21] F. Muñoz-Rojas *et al.*, Phys. Rev. B **74**, 195417 (2006); L. P. Zárbo and B. K. Nikolić, Europhys. Lett. **80**, 47001 (2007).
- [22] M. Wimmer, İ. Adagideli, S. Berber, D. Tománek, and K. Richter, unpublished.
- [23] We use a recursive Green's function algorithm as described in A. MacKinnon, Z. Phys. B **59**, 385 (1985).
- [24] O. N. Dorokhov, JETP Lett. **36**, 318 (1982); P. A. Mello, P. Pereyra, and N. Kumar, Ann. Phys. (NY) **181**, 290 (1988).
- [25] Eq. (20) in M. E. Gertsenshtein and V. B. Vasil'ev, Theor. Probab. Appl. **4**, 391 (1959); Eq. (4.3) in C. W. J. Beenakker and J. A. Melsen, Phys. Rev. B **50**, 2450 (1994).
- [26] P. W. Anderson *et al.*, Phys. Rev. B **22**, 3519 (1980).

- [27] C. W. J. Beenakker, Rev. Mod. Phys. **69**, 731 (1997).